Capture, ionization, and pair-production processes in relativistic heavy-ion collisions in the 1-GeV/nucleon energy range

A. Belkacem* and Harvey Gould†
Chemical Sciences Division, Building 71-259, Lawrence Berkeley National Laboratory, One Cyclotron Road, Berkeley, California 94720

B. Feinberg‡
Accelerator and Fusion Research Division, Building 80-101, Lawrence Berkeley National Laboratory, One Cyclotron Road, Berkeley, California 94720

R. Bossingham§
Nuclear Science Division, Building 50A-1148, Lawrence Berkeley National Laboratory, One Cyclotron Road, Berkeley, California 94720

W. E. Meyerhof‖
Department of Physics, Stanford University, Stanford, California 94305
(Received 27 March 1997)

The cross sections for capture, ionization, capture from pair production, and free pair production were measured for 0.96-GeV/nucleon U^{92+} and 0.405-, 0.96-, and 1.3-GeV/nucleon La^{57+} ions incident on Au, Ag, and Cu targets. The cross sections for capture from pair production, free pair production, ionization, and total capture (the sum of capture from pair production, radiative electron capture, and nonradiative capture) are analyzed as a function of collision energy, projectile, and target atomic numbers. We find that, when the collision energy is increased from 0.405 GeV/nucleon to 1.3 GeV/nucleon, the capture from pair production and the free pair production cross sections increase by almost a factor of 6, while the capture cross section decreases by two orders of magnitude. The ionization cross section is found to vary very weakly with the collision energy in the 1-GeV/nucleon energy range. We found a dependence of free pair production cross sections on the target and projectile atomic number to be close to Z^2, characteristic of an ionizationlike process. We also found a dependence of the capture from pair production cross sections on the target atomic number to be usually steeper than Z_t^2, and on the projectile atomic number, somewhat steeper than the Z_p^5, characteristic of a capturelike process. Theory and experiment are in some disagreement for capture from pair production, and free pair production, cross sections, but are in general agreement for the other capture processes and for ionization. [S1050-2947(97)06809-1]

PACS number(s): 34.70.+e, 25.75.−q

I. INTRODUCTION

In ion-ion or ion-atom collisions, charge changing occurs through ionization and electron capture. In our experimental situation, electron capture refers to the transfer of an electron from a stationary neutral target to a projectile ion. Two capture mechanisms contribute to this transfer: radiative electron capture and non-radiative electron capture. Radiative electron capture is the process in which an electron bound to the target is captured by the ion with the simultaneous emission of a photon to conserve momentum and energy. It differs from radiative recombination—which is the inverse of the photoelectric effect—in that in radiative recombination the electron is initially free. For radiative electron capture by (highly ionized high Z) relativistic ions, the binding energy of the target makes only a small contribution and radiative electron capture cross sections can be related to photoelectric cross sections. In nonradiative capture, energy, and momentum are conserved through momentum transfer by the projectile and target with no emission of a photon. In nonradiative capture there is often some relation between the collision energy and the binding energy of the state the electron is captured into.

At relativistic energies, the collision velocity is much greater than the Bohr velocity for all but the K-shell electrons of the heaviest elements, ionization cross sections are much larger than capture cross sections, and the equilibrium charge state of all projectiles is close to fully stripped. Theory and experiment for ionization, radiative electron capture, and nonradiative capture processes are generally in agreement [1–28] with a few interesting exceptions [29,30]. Measurements of a third relativistic charge changing mechanism, termed capture from pair production, or sometimes bound-electron free-positron pair production, has been reported [31,32]. The very large transient electromagnetic fields produced in the relativistic collision of the fast moving heavy ions result in high probabilities for electron-positron pair production [33–47]. Since heavy ions have large binding energies, the electron of the pair may be created directly bound to the ion, decreasing its charge state by one unit [48]. An extensive theoretical study of this process can be found in the literature [49–68].

*Electronic address: abelkacem@lbl.gov
†Electronic address: gould@lbl.gov
‡Electronic address: b_feinberg@lbl.gov
§Electronic address: rrbossingham@lbl.gov
‖Electronic address: fe.wem@forsythe.stanford.edu

The significance of electron capture from pair production is that it is a collision mechanism. Its cross section increases with increasing relativistic collision energy and, it becomes the dominant capture mechanism for highly relativistic ions in high-Z targets. It is the mechanism used in the production of antihydrogen [69]. Capture from pair production is also important, because it causes a limitation of the luminosity of RHIC, the relativistic heavy ion collider at Brookhaven National Laboratory, and LHC, the large hadron collider at CERN, the European Center for Nuclear Research [70]. In these machines, atomic collisions (without nuclear contact) between fully stripped ions may result in a charge change of one (or both) of the ions, changing their trajectory and effectively removing them from the beam.

In this paper, we present our measurements for electron capture, ionization, capture from pair production, and free pair production in the 1-GeV/nucleon energy range. Portions of this data have been reported in two letters [3,32]. In Sec. II, we present a discussion of radiative electron capture, nonradiative capture, capture from pair production, and free pair production. In Sec. III, we describe the experimental setup used at the Lawrence Berkeley National Laboratory's Bevalac to measure the cross sections for radiative electron capture, nonradiative capture, capture from pair production, and free pair production. In Sec. IV, we present our experimental results for each of the processes, and compare them with theory. We conclude with a summary.

II. ELECTRON CAPTURE, IONIZATION, AND PAIR PRODUCTION PROCESSES

The energy spectrum of an electron in the field of a nucleus consists of discrete bound states, a positive-energy continuum, and, in the Dirac picture, a negative-energy continuum. A neutral atom of atomic number Z consists of Z electrons occupying the discrete bound states and an infinite number of electrons occupying the negative-energy continuum. When a (bare) ion projectile impinges on this atomic target it may capture one of the bound state electrons or an electron from the negative-energy continuum. The capture of an electron from the negative-energy continuum leaves a hole in the negative-energy continuum which translates into the emission of a positron. Within this picture, capture and capture from pair production can be viewed as similar processes, with ordinary capture being the capture of a ''real'' electron initially in an atomic bound state, and capture from pair production being the capture of a ''virtual'' electron initially in the negative energy continuum. Capture from pair production is also treated theoretically as an excitation of an electron from the negative energy continuum of the *projectile* to one of its bound states. These two descriptions lead to the same result when a complete set of atomic states (negative- and positive-energy continuua) is used. A discussion of these two ways of treating capture from pair production, can be found in a recent paper by Ionescu and Eichler [71]. One should therefore expect to see both the ''excitationlike'' and ''capturelike'' behavior of capture from pair production in the dependence of its cross section on the collision energy, and on the target and the projectile atomic numbers. The energy, and the projectile and the target Z dependencies of the different cross sections are especially noticeable in the relativistic limit, which, although not fulfilled in our experiment ($\gamma \leqslant 2.5$, where γ is the Lorentz factor), do allow a simple qualitative discussion of the features of the theories. The experimental results will be compared to the appropriate theories in Sec. IV.

In the relativistic limit ($\gamma \gg 1$), almost all theories predict an approximate charge and energy dependence of nonradiative capture as [18,19,24]

$$\sigma_{\text{nonradiative capture}} \propto Z_p^5 Z_t^5 \gamma^{-1}, \tag{1}$$

where Z_p and Z_t are the atomic numbers of the projectile and the target, respectively. The dominant Z^5 dependencies arise in the nonrelativistic expression from the Fourier transforms of the bound-state wave functions of the target and the projectile atom. They reflect the ability of high-Z atoms to accommodate high-momentum components of the electron transitional motion.

If electron capture is accompanied by the emission of a photon, energy-momentum conservation does not require the initial electron wave function to possess high-momentum components in order to have sufficient momentum overlap with the moving projectile wave function. Capture of free electrons is no longer forbidden, and in the target atom, all Z_t electrons contribute to the cross section with about equal weight. Since the velocity of an electron capture into the projectile is that of a free electron as seen in the rest frame of the projectile, moving with the velocity spread within the target atom, the radiative electron capture cross section into the projectile varies as

$$\sigma_{\text{REC}} \propto Z_p^5 Z_t \gamma^{-1} \tag{2}$$

for large values of γ. Radiative electron capture to a specific state n can be written in terms of the photoelectric cross section as

$$\sigma_{\text{REC}}(n) = \sigma_{\text{PHO}}(n,k)[(\gamma-1)+B_n]^2/(\gamma^2-1), \tag{3}$$

where $\sigma_{\text{REC}}(n)$ is the radiative electron capture cross section in to principal quantum number n, $\sigma_{\text{PHO}}(n,k)$ is the photoelectric cross section for the n level for a photon of the energy of the electron seen by the moving ion, B_n is the binding energy of an electron in the n level in units of mc^2. A Z_p^5 dependence is contained in the photoelectric cross section.

For free pair production, in the limit of large values of γ, one may visualize the process in the center-of-mass frame as a creation process by two virtual photons, each of them contained in the rapidly time-varying electromagnetic field generated by moving nuclear charge Z_p or Z_t. Estimates for pair production give a cross section that varies roughly as [33,35]

$$\sigma_{\text{FPP}} \propto Z_p^2 Z_t^2 \ln^3(\gamma). \tag{4}$$

This cross section increases with energy. We find the same Z^2 dependence as in ionization and free pair production can be viewed as an ''ionizationlike'' process, where the initial state is an electron in the negative-energy continuum and the final state is that electron in the positive-energy continuum. The symmetry of the target and the projectile is stressed by the same atomic-number dependence with respect to both

partners. The increase with energy of the free pair production cross section comes from larger impact parameters that become available as the collision energy increases.

For capture from pair production, in which the electron is created in a bound state of the projectile (for example, a K shell), the factor Z_p^2 in expression (4) is replaced by the Z_p^5 dependence characteristic of capture into a bound state, as with nonradiative capture and radiative electron capture described above. The approximate dependence is [24]

$$\sigma_{\mathrm{CPP}} \propto Z_p^5 Z_t^2 \ln(\gamma). \tag{5}$$

Unlike radiative electron capture and nonradiative capture, the cross section of capture from pair production increases with increasing relativistic collision energy and becomes the dominant electron-capture process at highly relativistic energies.

In a more detailed recent calculation of capture from pair production, also in the relativistic limit, Baltz, Rhoades-Brown, and Weneser used a nonperturbative approach at small impact parameters, and a perturbative approach at large impact parameters, to establish a simple formula for capture from pair production cross section at very high energies [56–59],

$$\sigma_{\mathrm{CPP}} = A \ln\gamma + B. \tag{6}$$

The parameters A and B depend on Z_p and Z_t, but are independent of energy. The $A \ln\gamma$ term arises from the large impact parameter region of the interaction, with A entirely determined by perturbation theory and $\ln\gamma$ expressing the increasing impact parameter cutoff with increasing γ. The energy independent parameter B expresses both the perturbative and nonperturbative contributions at smaller impact parameters. Expressions (5) and (6) both display a $\ln\gamma$ dependence of the capture from pair production cross section at extreme relativistic energies.

The physical picture of the above discussion remains qualitatively correct at lower energies (1-GeV/nucleon range). But, as seen in Sec. IV, calculations for nonradiative capture, capture from pair production (and free pair production) in this energy region are required to reproduce experimental results quantitatively.

III. EXPERIMENTAL SETUP

The experiment was performed at the Berkeley National Laboratory's Bevalac accelerator using 0.4–1.3-GeV/nucleon La^{57+} and 0.96-GeV/nucleon U^{92+} projectiles on thin targets. Figure 1 shows a schematic of the beam line and the relative positions of the detectors. The heavy ion beam (La^{49+} or U^{68+}) is extracted from the Bevalac in a pulse with about a 1-s duration, and a repetition rate of 12 per minute. The beam passes through a stripping foil to produce the bare ions used for the experiment. Rates of between 10^3 and 5×10^6 heavy ions per pulse were used. The ions travel approximately 100 m from the extraction region of the accelerator to the last detector in vacuum of a few times 10^{-5} Torr to keep beam charge changing at negligible levels.

After passage through the target foil the beam is focused by a pair of quadrupole doublets and charge-state analyzed by a pair of dipole magnets (approximately 2 T m) to produce a horizontal focus of 0.4-cm full width at half maximum (5-cm vertical focus) and a typically 2-cm horizontal separation of adjacent charge states. Excellent charge-state separation is essential because only 0.1–2 % of projectile ions capture an electron in the thin-foil targets. With the target removed, we find that no more than a few parts per 10^4 of the bare ions are miscounted as a one-electron ion. This measurements is repeated during data taking and used to correct the data.

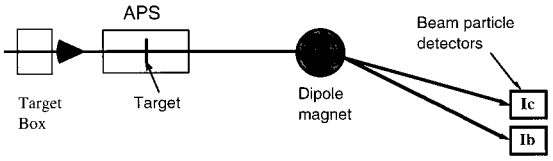

FIG. 1. Schematic of the beamline. The ions emerging from the target are charge state analyzed by a pair of large dipole magnets. Ib detects the bare ions, while Ic detects the one-electron ions. The advanced positron spectrometer (APS) detects the positrons and/or electrons emitted at the target. The target is located inside the APS shown in Fig. 2. See text for details.

The beam detector array uses three plastic scintillators, each coupled to a photomultiplier detector not shown in Fig. 1. One scintillator (Ib) is used to detect the bare projectile and the other (Ic) to detect the charge-changed one-electron ion. We verified systematically that the fraction of two-electron ions is negligible. A third detector (not shown) spans both charge states and is used as a check on Ib and Ic.

For the ionization and capture experiments, we used 10^3 ions per pulse to insure that the scintillators detect every single ion with an efficiency of unity. For pair production measurements, the beam intensity was increased above 10^5 per pulse to produce a signal rate of about one electron-positron pair per pulse. Two problems associated with high rates are beam pileup and scintillator darkening. Beam pileup occurs if two ions strike a scintillator within a time window that is shorter than the resolution time of the electronics, registering the two as a single event. In our setup, at a rate of 10^6 ions per pules, two ions strike a detector within 50 ns from each other 10% to 20% of the time. This value of beam pileup is tied closely to the microstructure of the beam, which in turn depends on the details of extraction of the beam from the accelerator. Beam pileup is negligible at low rates. We measure the ratio of Ic to Ib at low intensities, where Ib is not affected by beam pileup, and then systematically monitor that ratio at high rates. Ic is struck only by the small fraction of the beam that has capture an electron, and thus counts every ion with an efficiency of unity, even at high beam intensities.

The second problem associated with high beam intensity is scintillator darkening which is physical damage to the plastic at the location of the beam trajectory. It develops over hours or days, depending on the beam intensity and the atomic number of the projectile. Darkening can affect the pulse height and thus the counting efficiency and timing of the detector. Darkening is monitored by checking the analog output signal of the photomultiplier tube attached to the scintillator. Similar to beam pileup, darkening is also monitored by checking the ratio of Ic to Ib.

Two sets of targets are used for measurements. A target

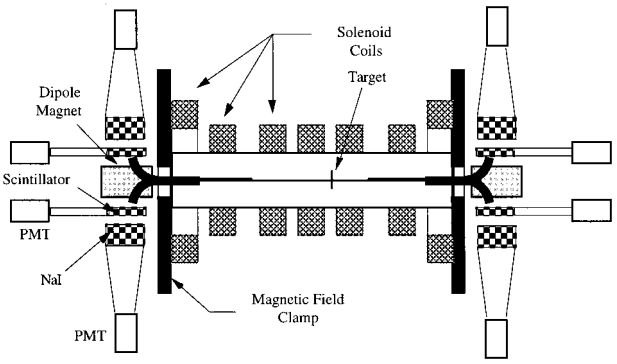

FIG. 2. Schematic diagram of the advanced positron spectrometer (sectional view from the top). The solenoidal field decreases adiabatically from the target toward the ends, causing the divergence of the electrons and positrons to decrease, allowing them to be swept by the dipole magnets into the scintillator detectors. The target, or a calibration source, is located near the center of the solenoid. The heavy ion beam travels horizontally through the center of the apparatus.

changer with 49 targets which can be inserted in any combination is used for measurements of total capture cross sections and ionization cross sections. For capture from pair production and free pair production, it is necessary to detect the positron emitted from the target. In the present setup, the targets are mounted on a target ladder inside the advanced positron spectrometer (APS). We use Au, Ag, Cu, and mylar targets with thicknesses ranging from 0.1 to 5.1 mg/cm^2. These thicknesses are chosen to keep the probability for stripping a captured electron to less than 20%. The target thicknesses are determined to $\pm 10\%$ by measuring the energy loss of α particles emitted by an ^{241}Am source.

The advanced positron spectrometer, shown in Fig. 2, is configured in such a way that it measures the energy and the angular distribution of the electrons and the positrons emitted at the target. The APS is 2.6 m long and consists of a solenoid with a dipole magnet at each end. The solenoid is constructed from seven coils that are powered independently to generate a longitudinal field that is strong ($B = 0.8$ T maximum) at the target foil in the APS, but adiabatically decreases to reach a value of about 0.2 to 0.25 T at each end. Figure 3 shows a profile of the longitudinal field generated by the solenoid and the transverse field generated by the dipoles. The adiabatically decreasing longitudinal magnetic field transports the electrons and positrons away from the target, and, most importantly, converts much of their transverse motion into longitudinal motion using the particle's cyclotron frequency as an adiabatic invariant.

At each end of the solenoid the longitudinal field is sharply reduced to zero within a few cm, using a magnetic-field clamp consisting of a 12-cm-diameter exit hole in a 5-cm-thick steel end plate. The positrons and the electrons which transform their transverse momentum into longitudinal momentum as a result of the adiabatic decrease in field are deflected in opposite directions by the transverse dipole field into their respective detectors. In addition to the very clean separation of electrons and positrons, this careful shaping of the magnetic field allows a very high and very uniform acceptance.

Tests of the apparatus using radioactive sources and

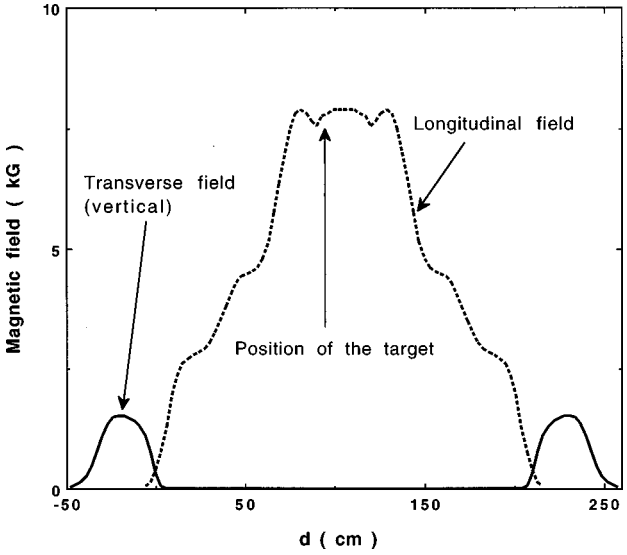

FIG. 3. Measured longitudinal magnetic field (dashed line) inside the APS solenoid and transverse magnetic field (solid lines) of the dipole magnets located at each end of the solenoid. For better access the target is located slightly upstream from the center of the solenoid.

knock-on electrons ejected by ion beams from fixed solid targets show an acceptance close to unity for emission angles of up to 75° forward and backward. This acceptance is independent of the electron or positron energy in the energy range investigated (from 0.1 to 3 MeV). The high acceptance is not very sensitive to the exact shape of the field shown in Fig. 3, and the current in each coil can be varied by as much as 10% without any noticeable change in acceptance. The acceptance decreases by more than 30% if the adiabaticity is not used, and this loss comes preferentially from electrons (or positrons) emitted at large angles. Without the adiabatically decreasing field, most of the positrons emitted at large angles, upon reaching the end of the solenoid field, would have a large transverse momentum, causing them to strike the walls of the apparatus before they can be deflected into the spectrometer detectors.

The initial discrimination between electrons and positrons is made by the dipole magnets that deflect electrons and positrons in opposite directions into their respective detectors. These detectors consist of four, 10-cm-high, 15-cm-long, and 1.9-cm-thick plastic scintillators, two upstream, to detect the backward positrons and electrons, and two downstream, to detect the forward positrons and electrons.

At 1 GeV/nucleon, a large number of knock-on electrons are ejected from the target by the collisions with high-Z projectile ions. For a 1-mg/cm^2 Au target, approximately 3–4 electrons, with an energy above 100 keV, are ejected for every collision with a U^{92+} ion, while only a few positrons are expected for every million collisions. Roughly 0.2–0.3 % of these knock-on electrons backscatter from the electron scintillator into the positron scintillator, simulating a positron. The discriminate against these scattered electrons, we require the detection of one of two 511-keV photons that are emitted back to back when the positron comes to rest and annihilates in the plastic scintillator. The 511-keV photons are detected by NaI scintillation detectors (12.5-cm diameter and 15 cm long) directly behind each of the four plastic

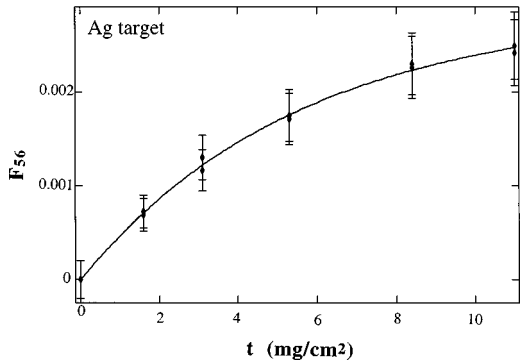

FIG. 4. Fraction of La^{56+} as a function of target thickness for a 1.3-GeV/nucleon La^{57+} projectile incident on Ag targets. The solid curve is a fit to the data based on Eq. (7).

scintillator detectors. The 511-keV photon easily passes through the thin low-Z plastic scintillator. The detection efficiency of the NaI detector for the 511-keV photons is measured to be 42%, with approximately 60% of the detected photons appearing as the narrow single peak with an 8% energy resolution and the remainder as a broad Compton distribution. In our data analysis, only the photopeak is used to discriminate against background (gamma) photons in accidental coincidence with backscattered electrons. These background gammas come from activation by the beam of the beamline, cave, and apparatus.

For positrons of equal energy, the ones emitted at larger angles will take longer to traverse the solenoid than one emitted at a smaller angle. A measurement of the time-of-flight of each detected positron through the strong field of the solenoid, combined with its measured energy is used to determine its emission angle with respect to the beam direction.

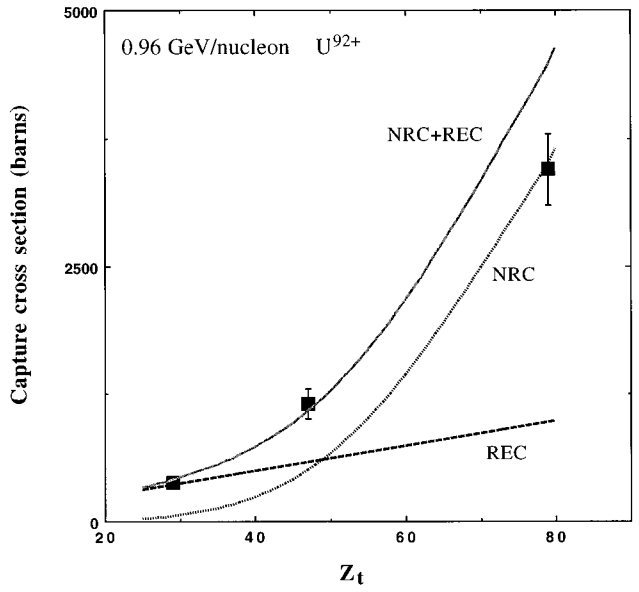

FIG. 5. Measured total electron-capture cross section (radiative electron capture, plus nonradiative capture, plus capture from pair production) as a function of target atomic number for 0.96-GeV/nucleon U^{92+} (on Au, Ag, and Cu targets). The theoretical predictions for nonradiative capture and radiative electron capture are shown in long-dashed and short-dashed lines, respectively, and the sum as a solid line.

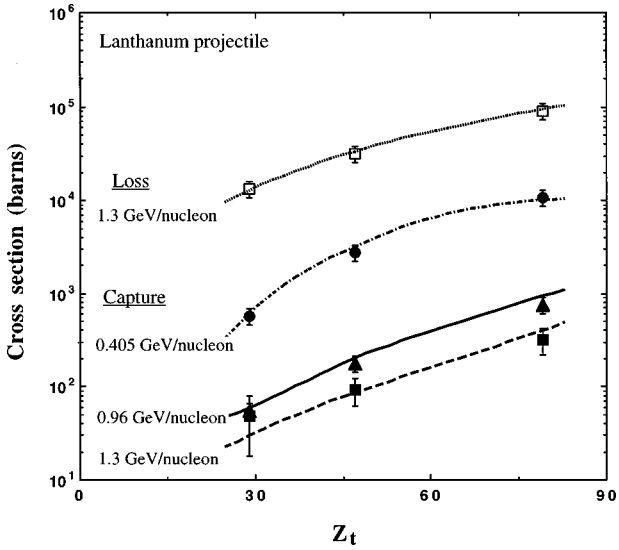

FIG. 6. Measured total electron-capture cross section for 0.405-, 0.96-, and 1.3-GeV/nucleon La^{57+} and electron loss cross section for 1.3-GeV/nucleon La^{56+} as a function of target atomic number. The solid lines and the dashed curves are theoretical values (see text for details) and, for capture, include contributions from radiative electron capture and nonradiative capture.

The four fast-timing scintillator-photomultiplier detectors are used to measure the energy and the time of flight of the positrons and the electrons. The energy resolution is approximately 17%, and the time resolution is 150–200 ps which translates into an angular resolution of 15° or better. The timing reference for the positron is given by the ion that produced the positron, detected by the fast-timing scintillator-photomultiplier detector Ic or Ib (Fig. 1).

IV. RESULTS AND DISCUSSION

A. Capture and ionization

The cross section for capture of a target electron by the projectile is obtained by measuring the fraction of one-electron ions emerging from the target when a beam of bare ions is incident on the target. This fraction is measured for several target thicknesses, with the thicknesses chosen to insure that the measurements lie in the linear part of the target thickness dependence curve. For some target materials, the thicknesses are varied over a wide range to allow the extraction of the electron loss cross section as well. Figure 4 shows the fraction of La^{56+} (one-electron) ions as a function of target thickness for 1.3-GeV La^{57+} projectiles impinging on Ag. The solid line is a least squares fit to the data and reflects electron capture and loss while the projectile ion travels inside the target. Since only bare ions and one-electron ions are of importance at these energies, the fitting function is simply given by [72]

$$F_{56}=[\sigma_c/(\sigma_c+\sigma_1)]\{1-\exp[-(\sigma_c+\sigma_1)x]\}, \qquad (7)$$

where F_{56} is the fraction of one-electron ions, σ_c and σ_1 are the capture and loss cross sections in cm^2, respectively, and x the target thickness in atoms/cm^2. The fraction F_{56} reaches an equilibrium value of $\sigma_c/(\sigma_c+\sigma_1)\approx\sigma_c/\sigma_1$ at very large thicknesses. At 1.3 GeV/nucleon, the ionization cross section

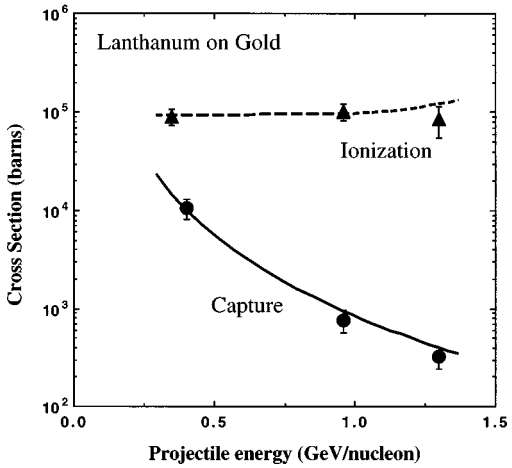

FIG. 7. Measured total electron-capture cross section for La^{57+} on Au and electron loss cross section of La^{56+} on Au, both as a function of collision energy. The solid lines and the dashed curves are theoretical values (see text for details) and, for capture, include contributions from radiative electron capture and nonradiative capture.

is much larger than the capture cross section, by a factor of approximately 300 for the case of La^{57+} on Ag, as shown in Fig. 4.

In Figs. 5–7, our experimental values of the ionization and total capture cross sections, are compared with theoretical predictions of radiative electron capture, nonradiative capture, and ionization. The theoretical numbers for capture include contributions from all the excited states of the target and the projectile. For ionization, the theoretical values only include the electron loss from the projectile ground state because, in our experimental conditions, the mean free path between two successive collisions is much longer than the radiative decay of excited states to the ground state. At these energies, capture from pair production does not make a significant contribution to the total capture cross section. Radiative electron capture differs only slightly from radiative recombination, which is the inverse of the photoelectric effect and can be calculated from the photoelectric cross section. For radiative electron capture, the electron binding in the target gives rise to a momentum spread which is usually taken into account by the Compton profile. Radiative electron capture is calculated using Eq. (3) with photoelectric cross sections from Hubbell [73]. The photoelectric cross sections are those emitted photons whose energy is equal to the binding energy of the capture electron plus the kinetic energy of the captured electron seen in the rest frame of the projectile.

Two-center coupled-channel calculations for nonradiative capture [22] provide the best agreement with experiment for high-Z projectiles in the 1-GeV/nucleon energy range. However, these calculations are extremely time consuming and are not practical at present to study a large number of collision systems. Eikonal calculations are more commonly used for nonradiative capture. Theoretical values used in this paper were calculated by Eichler and Ichihara using a similar procedure as in Ref. [9]. In particular they used the ''post form'' for the U^{92+} projectile and the ''prior form'' for the La^{57+} projectile. For ionization, plane-wave Born approximation values which include screening and antiscreening are taken from Anholt and Becker [24].

1. Target and projectile atomic number dependence

Figure 5 shows the total capture cross section measured for 0.96-GeV/nucleon U^{92+} on Cu, Ag, and Au targets. The measured cross section is a combination of radiative electron capture and nonradiative capture and includes capture into excited states. Also shown in Fig. 5 are the theoretical predictions for radiative electron capture and nonradiative capture. The sum of these agrees well with the measured cross sections for Cu and Ag targets but overestimates the cross section for a Au target by 20%. The discrepancy between theory and experiment for high-Z targets may be due to limitations of the eikonal calculations. Indeed, using the prior and post form expressions, the eikonal calculations treat the lightest of the two ions perturbatively, which in the present case would be the Au target.

Radiative electron capture is the dominant capture mechanism for low-Z targets while nonradiative capture dominates for high-Z targets. Qualitatively, this means that electrons loosely bound in low-Z target atoms (or in outer shells of high-Z atoms) are more likely to be captured with photon emission than without.

Figure 6 shows capture and loss cross sections measured for a La^{57+} projectile at 0.405, 0.96, and 1.3 GeV/nucleon. There is a good agreement between theoretical and experimental values both for capture and loss. The loss cross section at 1.3 GeV/nucleon is 2–3 orders of magnitude larger than the capture cross section.

2. Energy dependence

Figure 7 shows the cross sections for capture and loss for La^{57+} on Au as a function of the projectile energy. As expected, the capture cross section decreases very rapidly with increasing projectile energy, in good agreement with theory. We find that the capture cross section falls approximately as γ^{-3}, much faster than the γ^{-1} dependence given by the relativistic-limit expressions (1) and (2). The loss cross section varies very little with collision energy in the 1-GeV/nucleon energy range, in agreement with theory. At the highest collision energy, the measured ionization cross section appears to be slightly, but not significantly, smaller than the theoretical value.

The energy dependence of the capture cross sections for other targets can also be seen from Fig. 6. The capture cross sections decrease very rapidly with increasing projectile energy for all targets, and shrink by 1–2 orders of magnitude between 0.405 and 1.3 GeV/nucleon. Overall, we find that, in the 1-GeV/nucleon energy range, theory is usually capable of predicting qualitatively as well as quantitatively (within 20%) the measured cross sections for capture and loss.

B. Capture from pair production and free pair production

Unlike nonradiative capture and radiative electron capture, capture from pair production, and free pair production are accompanied by the emission of a positron. The detection and the measurement of the energy and momentum of the

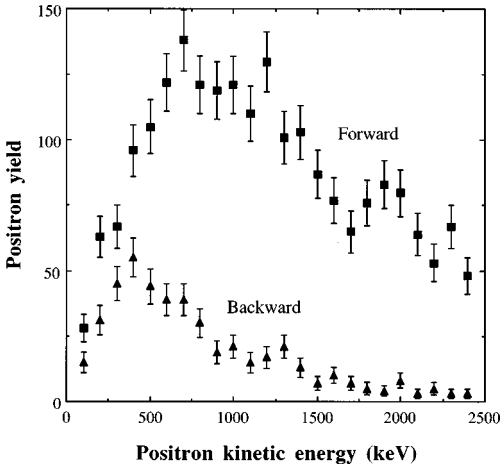

FIG. 8. Measured positron energy spectrum for electron capture from pair production by 0.96-GeV/nucleon U^{92+} on a Au target. Each data point is the result of an integration over all angles between 0° and 75° (forward and backward with respect to the beam direction) and over an energy interval of 100 keV.

emitted positron can be considered as a signature of the initial state that the electron occupied in the negative energy continuum.

1. Positron energy and angular distributions

Figure 8 shows the positron energy spectra for capture from pair production for a 0.96-GeV/nucleon U^{92+} beam incident on a 1-mg/cm^2 Au target. The data for the forward and backward directions have been integrated over emission angles of 0° to 75° and 105° to 180°, respectively. The two spectra are taken simultaneously, and therefore are normalized to the same number of incident uranium ions. The spectra show a relative lack of low-energy positrons. This is due to the repulsion of the positrons by the gold target nuclei which are at rest in the laboratory frame. The forward positron energy spectrum displays a broad maximum around 800 keV, while the backward spectrum displays a maximum around 400 keV.

Figure 9 shows the positron energy spectrum for capture

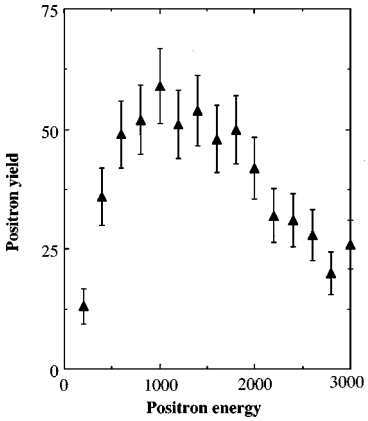

FIG. 9. Measured positron energy spectrum for electron capture from pair production by 1.3-GeV/nucleon La^{57+} on a Au target. Each data point is the result of an integration over all angles between 0° and 75° (forward) with respect to the beam direction and over an energy interval of 200 keV.

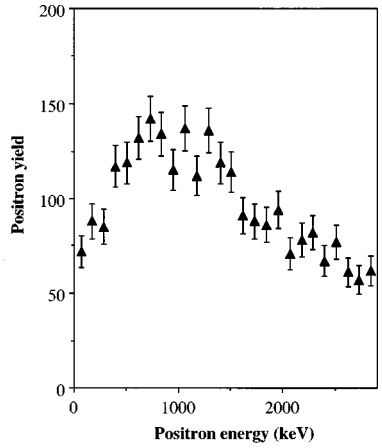

FIG. 10. Measured positron energy spectrum for free pair production by 1.3-GeV/nucleon La^{57+} on a Au target. Each data point is the result of an integration over all angles between 0° and 75° (forward) with respect to the beam direction and over an energy interval of 120 keV.

from pair production, measured with the forward detector for 1.3-GeV/nucleon La^{57+} on Au. We find the same features as Fig. 8. Figure 10 shows the positron energy spectrum for free pair production for 1.3-GeV/nucleon La^{57+} on Au. The free pair production positron spectrum, recorded with the forward positron detector, displays the same general features as the capture from pair production positron spectrum shown in Figs. 8 and 9. The signature of the free pair production process is the simultaneous detection of a positron emitted at the target and a La^{57+} (bare ion) in detector Ib (Fig. 1). Since a free pair production event has one coincidence requirement less than capture from pair production (in which a charge change is required—a relatively rare event), there is a higher probability of miscounting a scattered low-energy electron as a positron. These false events (if they occur) are most likely to populate the very low-energy part of the spectrum, and are the likely reason for the smaller suppression of the low-energy positrons in Fig. 10 compared to Figs. 8 and 9.

Figure 11 shows the positron spectrum for capture from pair production, recorded with the forward detector, for 0.96-

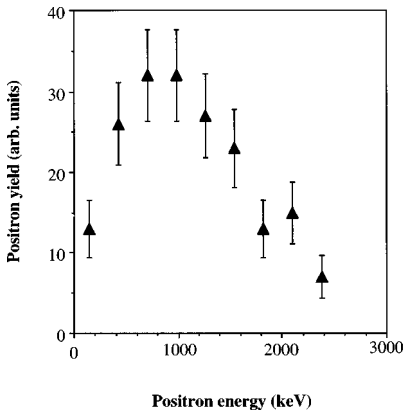

FIG. 11. Measured positron energy spectrum for electron capture from pair production by 1.3-GeV/nucleon La^{57+} beam on Cu. Each data point is the result of an integration over all angles between 0° and 75° (forward) with respect to the beam direction and over an energy interval of 300 keV.

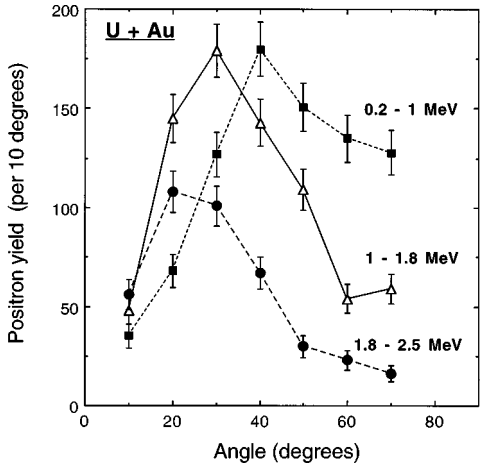

FIG. 12. Yield of positrons as a function of positron emission angle with respect to the beam direction for positron kinetic energies between 0.2–1, 1–1.8, and 1.8–2.5 MeV, respectively. Each data point is the result of an integration over an angular interval of 10°. The data are for 0.96-GeV/nucleon U^{92+} on Au.

GeV/nucleon U^{92+} on Cu. Comparing this spectrum with the previous spectra shows that, with the present choice of energies and projectiles, the target atomic number has little or no effect on the shape of the positron spectrum.

As already seen in Fig. 8, the high-energy electrons are emitted preferentially in the forward direction. This relation is seen more clearly in Fig. 12, which shows the measured yield of positrons as a function of the positron emission angle with respect to the beam direction, for different positron energies, for 0.96-GeV/nucleon U^{92+} on Au. The positrons with kinetic energies higher than 1.8 MeV are emitted preferentially at angles smaller than 40°, while positrons with energies lower than 1.0 MeV are emitted preferentially at the larger angles. This angular dependence agrees qualitatively with predictions based on first order-perturbation theory for capture from pair production calculated by Becker [63]. Figure 13 gives the angular distribution of the positrons integrated over all positron kinetic energies between 100 keV and 2.5 MeV. There is a strong maximum in the distribution between 30° and 45°, which is roughly $1/\gamma$ rad, and is assumed to be largely kinematic. The two parts of the spectrum from 0° to 75° and from 105° to 180° were recorded simultaneously. A smooth continuation from one part of the spectrum to the other is found. Below, this smooth continuating is used to estimate the fraction of the total cross section not detected by the APS.

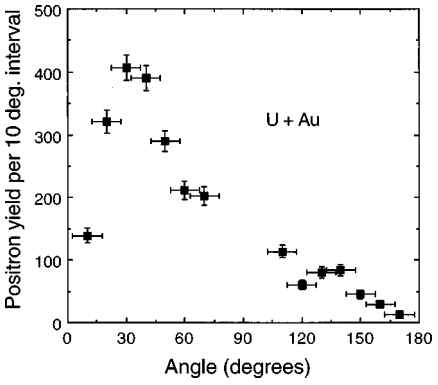

FIG. 13. Total yield of positrons as a function of positron emission angle with respect to the beam direction. Each data point is a result of an integration over all positron kinetic energies between 0.1 and 2.5 MeV. The data are for 0.96-GeV/nucleon U^{92+} on Au.

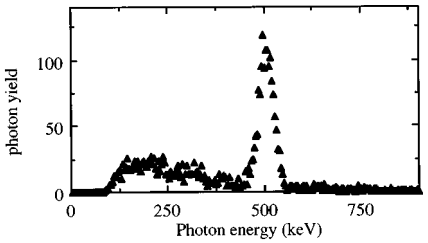

FIG. 14. Photon energy spectrum in the NaI detector set behind the forward positron detector. The spectrum shown here is for capture from pair production by 0.96-GeV/nucleon U^{92+} on Au.

2. Total positron cross sections and corrections

To obtain total cross sections from positron spectra, one has to integrate over the positron energy (and angle) and correct for the angular region not covered by the spectrometer and for γ detector efficiency. (Since only events that register a 511-keV γ are used in our analysis, it is necessary to correct the cross sections for the solid angle of the NaI detector and its efficiency.) A straightforward way to obtain the total cross section is to count the number of 511-keV photons. Figure 14 shows a typical photon spectrum in the NaI detector set behind the forward positron detector (Fig. 2), for capture from pair production (U^{92+} on Au). The spectrum displays the 511-keV photopeak and a broad Compton distribution. In general, some unwanted γ background from various beam-activated sources in the experimental area populates the lower part of the spectrum, and contributes to the Compton distribution. We use only the photopeak, corrected for detection efficiency, to determine the total cross section.

We correct for the undetected angular region between 75° and 105° in the spectrometer, using the positron angular distribution for capture from pair production, shown in Fig. 13. Since our focus during this experiment was on capture from pair production, we did not record enough statistics to obtain an equivalent positron angular distribution for free pair production. However, the positron angular distributions for capture from pair production and for free pair production are expected to be similar, allowing us to apply the same corrections. The correctness of this assumption is supported by the fact that the ratio of positrons detected in the backward direction to positrons detected in the forward direction is found to be the same for capture from pair production and for free pair production. Furthermore, since the fraction of positrons not detected by the APS is small, we believe that the resulting error we make is well within our overall error estimate.

The data are also corrected for the contribution from false events corresponding to two-step processes: (i) capture from pair production followed by stripping of the electron in the target which simulates free pair production; (ii) free pair production followed by capture of a target electron, which simulates capture from pair production. The (positive or negative)

contribution from the first two-step process is corrected by using well-known ionization cross sections (in most cases measured during the same experiment), and are reduced to minimal values by using very thin targets. The second two-step process is more difficult to estimate accurately, because it is dominated by the two-step process occurring in the same collision. This background is larger in collision systems where nonradiative capture probabilities are large, at lower collision energies and high-Z targets. Using theoretical values of capture probabilities for small impact parameters [18,22,52], where pair production preferentially occurs, we estimate that false events contribute at most 6% to capture from pair production for U^{92+} on Au. The contribution is smaller for Ag and Cu targets.

We find the total cross section for capture from pair production and free pair production of 0.96-GeV/nucleon U^{92+} on Au to be 2.19 ± 0.25 and 3.3 ± 0.65 b, respectively. A calculation of capture from pair production, based on first-order perturbation theory, and summed over all possible final bound states, yields a value of 1.01 b, which is lower than our measured cross section by a factor of ~ 2.2. A nonperturbative coupled-channels calculation of capture from pair production has been published for Pb on Pb at 1.2 GeV/nucleon by Rumrich *et al.* [50]. Using scaling from perturbation theory to extrapolate those results to U on Au gives a value which is higher than our measured cross section by a factor of ~ 2. Baltz, Rhoades-Brown, and Weneser [57] noted that the small basis set used by Rumrich *et al.* gives rise to a gauge dependence. A more recent nonperturbative result based on the solution of the time-dependent Dirac equation in momentum space predicts a value of 2.6 b for U^{92+} on Au [52]. However, this good agreement with the experimental value is overshadowed by a large uncertainty in the numerical result.

Discrepancies between theory and experiment are found for free pair production as well. Using first-order perturbation theory, but different expressions for the target wave functions, Becker, Grun, and Scheid [35] predicted a value of 5.1 b, and Decker [34] a value of 1.25 b. These different numbers (which both disagree with our measured cross section) are obtained from a similar perturbation theory, and thus highlight some of the difficulties encountered in free pair production calculations. Unlike capture from pair production, where there is only one final state, for example, the K shell, free pair production involves an infinite number of final states for the electron, making the calculations very tedious.

3. Target and projectile atomic number dependence

An important feature of capture from pair production and of free pair production is the dependence of their cross section on the atomic number of the target and projectile. Figure 15 shows the total cross section of capture from pair production and free pair production (both scaled by Z_t^2) for 1.3-GeV/nucleon La^{57+} on Au, Ag, and Cu targets. A Z_t^2 dependence is represented by the horizontal lines in the figure. We find that the free pair production cross section follows a Z_t^2 dependence, while the capture from pair production cross section has a slightly stronger dependence as evidenced by

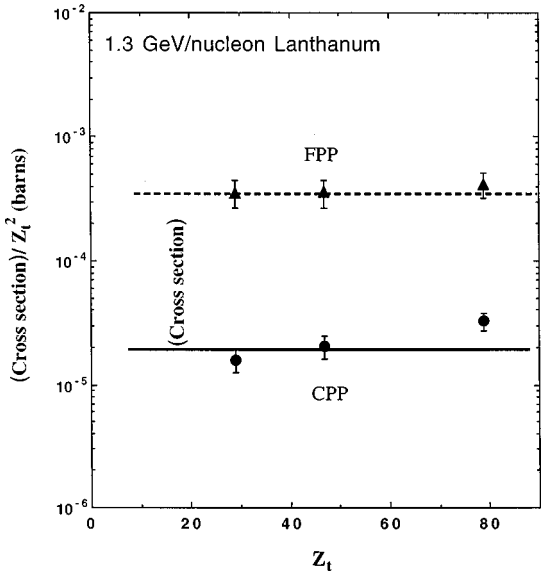

FIG. 15. Capture from pair production and free pair production cross sections, divided by Z_t^2, as a function of the target atomic number for a 1.3-GeV/nucleon La^{57+} projectile. The horizontal lines are a guide for the eye to highlight a Z_t^2 dependence.

the positive slope. A fit to the data shown in Fig. 15 gives $Z_t^{2.15\pm0.25}$ for free pair production and $Z_t^{2.95\pm0.4}$ for capture from pair production.

Figure 16 compares the Z_t dependence of capture from pair production, for two different projectiles (La^{57+} and U^{92+}) at 0.96 GeV/nucleon. (This data are not scaled by Z_t^2.) The slopes of the two sets of data are very similar. We find a $Z_t^{2.65\pm0.35}$ for the La^{57+} projectile and a $Z_t^{2.8\pm0.25}$ for U^{92+} projectiles. It appears that in 1-GeV/nucleon energy range, capture from pair production exhibits a Z_t dependence closer to Z_t^3 than to Z_t^2, regardless of projectile or collision energy, while free pair production follows a Z_t^2 dependence. We suggest that the stronger dependence for capture from pair production could be due to a higher effective binding energy while the two nuclei are close together. If this suggestion is correct, one expects the effect to diminish at higher energies since the total cross section should be dominated by

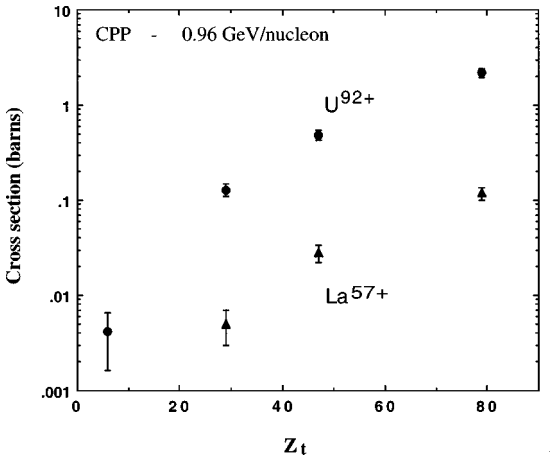

FIG. 16. Capture from pair production cross sections measured for 0.96-GeV/nucleon U^{92+} and La^{57+} projectiles as a function of target atomic number.

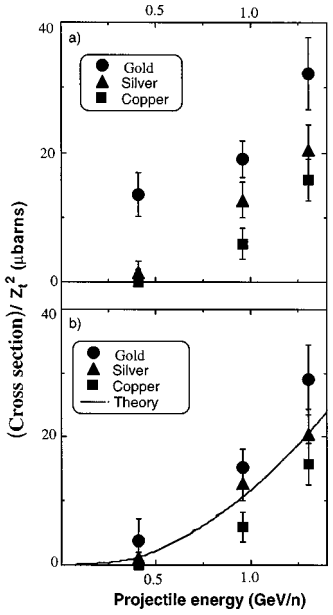

FIG. 17. (a) Cross sections (divided by Z_t^2) for electron capture in coincidence with the detection of a positron for La^{57+} incident on Au, Ag, and Cu targets. These cross sections are a sum of capture from pair production and false events due to free pair production along with the capture of a target electron. (b) Data in (a) corrected for false events (see text). Calculations based on first-order perturbation theory are shown as a solid line.

the increasing contribution from large impact parameters.

The capture from pair production cross section for 0.96-GeV/nucleon U^{92+} projectiles is found to be approximately 20 times larger than the cross section for 0.96-GeV/nucleon La^{57+} projectiles, for all targets. This means that the cross section depends more strongly on the projectile atomic number than it does on the target atomic number. Using the U and La data, we find a dependence on projectile atomic number that is $Z_p^{6.54\pm0.65}$ (for a Au target), compared to a target atomic number dependence between Z_t^2 and Z_t^3. In contrast, the free pair production cross section varies as $Z_p^{1.53\pm0.8}$ for the Au target, which is very close to its dependence on the target atomic number. Again, for capture from pair production, the stronger projectile atomic number dependence than Z_p^5, expected at the relativistic limit, may be due to a higher effective binding energy while the two nuclei are in close proximity. The above Z_t and Z_p dependencies for free pair production are in general agreement with the dependencies expected at the relativistic limit, but for capture from pair production, are both somewhat stronger.

4. Energy dependence

Another important feature of capture from pair production and free production is the dependence of their cross sections on the collision energy. Figure 17 shows in (a) the uncorrected and in (b) the corrected capture from pair production cross sections (divided by Z_t^2) for 0.405-, 0.96-, and 1.3-GeV/nucleon La^{57+} projectiles on Au, Ag, and Cu targets. This cross section increases rapidly with increasing collision energy. In contrast, the cross section for capture of a target electron (Fig. 7) decreases rapidly with increasing collision energy.

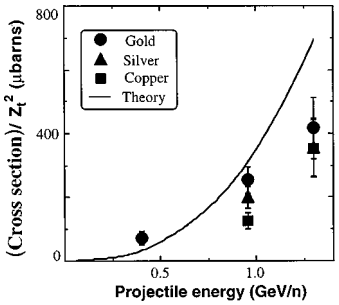

FIG. 18. Free pair production cross section (divided by Z_t^2) for La^{57+} incident on Au, Ag, and Cu targets as a function of the La^{57+} projectile energy. Calculations based on first-order perturbation theory are shown as a solid line.

For La, Fig. 17(a), we estimate that at least two-thirds of the events measured at 0.405 GeV/nucleon for a Au target are due to free production followed by capture of a target electron. If one makes the extreme assumption that all these events are false, then an upper limit on the contributions of these false events to capture from pair production in the Au target at 0.96 and 1.3 GeV/nucleon is 20% and 10%, respectively. Figure 17(b) shows the capture from pair production cross sections with these corrections for the background. The corrections are negligible for the low-Z targets at all three energies, and very small for high energies, due to the small nonradiative capture cross sections (see Fig. 6). The correction increases the apparent dependence of the cross section on collision energy. Figure 17(b) also shows the results of a calculation based on first-order perturbation theory [63]. This calculation (which yields a Z_t^2 dependence) includes the contribution of the excited states of the projectile to the total cross sections. We find that, in the energy range studied here, there is fair agreement between theory and experiment for the cross sections and their energy dependence.

Figure 18 shows the free pair production cross section as a function of energy for La^{57+} on Au, Ag, and Cu targets. Similar to capture from pair production, the cross section is found to increase rapidly with increasing collision energies. Also shown is a first-order perturbation theory calculation of the free pair production cross section as a function of energy [35]. Here the perturbation calculation overestimates the measured values at the higher projectile energies. There are large uncertainties at 0.405 GeV/nucleon for capture from pair production, and the limited range of energies studied here make it difficult to confirm the prediction that free pair production increases faster with increasing collision energy than capture from pair production. The experimental cross sections for capture from pair production and free pair production rise with energy closer to $\ln^2\gamma$ than the $\ln\gamma$ dependence expected at the relativistic limit.

V. SUMMARY AND CONCLUSION

This paper presents a summary of our data on capture, ionization, capture from pair production, and free pair production, for bare uranium and lanthanum projectiles in the 1-GeV/nucleon energy range. The cross sections were measured as a function of the collision energy, the target atomic number, and the projectile atomic number. Among important features, we find that the total capture cross section (domi-

nated by nonradiative capture and radiative electron capture) decreases almost as γ^{-3}, while the capture from pair production cross section increases almost as fast as $\ln^2\gamma$, still far from the respective expected relativistic limits of γ^{-1} and $\ln\gamma$. At higher energies, the capture from the pair production cross section is expected to become larger than the capture cross section of a target electron. We also find that, in the 1-GeV/nucleon collision energy range studied here, free pair production does not rise much faster than capture from pair production. Again this is very different from the relativistic limit where, for example at RHIC energies, the free pair production cross section is expected to be several orders of magnitude larger than the capture from the pair production cross section. Measurements performed by the E892 Collaboration at the Brookhaven National Laboratory's AGS at 10 GeV/nucleon, and being currently analyzed, will likely address this interesting question.

A series of papers describing measurements and calculations of nonradiative capture, radiative electron capture, and ionization in an energy range close to the one studied here have been published previously [1–7]. For similar systems (U on Au, for example) our results for capture and ionization are very close to the measurements reported by these authors.

We find that existing theories reproduce well the measured capture and loss cross sections. We find a small discrepancy (about 20%) between the calculated capture cross section and the measured capture cross section for U^{92+} on Au. We suggest that this discrepancy is a result of the limitations of the eikonal calculations for a high-Z projectile on a high-Z target.

Unlike capture and ionization, capture from pair production and free pair production data are not well reproduced by present theory. Both perturbative and nonperturbative methods that describe capture from pair production in the 1-GeV/nucleon energy range can be found in the literature. In practice, only theories based on first-order perturbation theory or equivalent photon methods can be used for direct comparison with our experimental data. The results of these calculations disagree with our data by a factor of 2 or more for the heaviest systems. This suggests that these collision systems are highly nonperturbative. Nonperturbative calculations, however, are computationally intensive and presently have large numerical uncertainties due to the limitations of CPU time or memory available on the fastest computers. Finally, many of the calculations are performed in the relativistic limit of the collision energy, and do not apply quantitatively to the present data. Experiments at higher energies are needed to test these calculations.

ACKNOWLEDGMENTS

We thank Steven Abbott for the engineering design of the Advanced Positron Spectrometer, Richard Leres for the data-acquisition software development, and Harvey Oakley and the Bevalac technical support staff for helping put together the experiment in record time to meet the deadline set by the shutdown of the Bevalac. We thank Donald Jourdain and Cory Lee for helping us design and build very efficient scintillating detectors, and Don Syverstrud and James Dougherty for helping to assemble the advanced positron spectrometer. We thank Charles Munger and Lynette Levy for their assistance during the data taking, and we thank Klaus Momberger for fruitful discussions about the theory of capture from pair production. We thank P. Joerg Eichler for the many fruitful discussions about nonradiative capture and radiative electron capture, and especially for kindly taking the time to rerun some of his computer codes to provide us with the theoretical values for capture used in this paper. This work was supported by the Director, Office of Energy Research, Office of Basic Energy Sciences, Division of Chemical Sciences, of the U.S. Department of Energy (DOE) under Contract No. DE-AC-03-76SF00098. One of us (B.F.) was supported by the Office of High Energy and Nuclear Physics, Division of Nuclear Physics, of the U.S. DOE. One of us (W.M.) was partially supported by NSF Grant No. PHY8614650.

[1] R. Anholt, S. A. Andriamonje, E. Morenzoni, Ch. Stoller, J. D. Molitoris, W. E. Meyerhof, H. Bowman, J.-S. Xu, Z.-Z. Xu, J. O. Rasmussen, and D. H. H. Hoffmann, Phys. Rev. Lett. **53**, 234 (1984).

[2] H. Gould, D. Greiner, P. Lindstrom, T. J. M. Symons, and H. Crawford, Phys. Rev. Lett. **52**, 180 (1984).

[3] R. Anholt, W. E. Meyerhof, Ch. Stroller, E. Morenzoni, S. A. Andriamonje, J. D. Molitoris, O. K. Baker, D. H. Hoffmann, H. Bowman, J.-S. Xu, Z.-Z. Xu, K. Frankel, D. Murphy, K. Crowe, and J. O. Ramussen, Phys. Rev. A **20**, 2234 (1984).

[4] R. Anholt, W. E. Meyerhof, H. Gould, C. Munger, J. Alonso, P. Thieberger, and H. E. Wegner, Phys. Rev. A **32**, 3302 (1985).

[5] W. E. Meyerhof, R. Anholt, J. Eichler, H. Gould, C. Munger, J. Alonso, P. Thieberger, and H. E. Wegner, Phys. Rev. A **32**, 3291 (1985).

[6] R. Anholt, W. E. Meyerhof, X.-Y. Xu, B. Feinberg, R. J. McDonald, H. E. Wegner, and P. Thieberger, Phys. Rev. A **36**, 1586 (1987).

[7] W. E. Meyerhof, R. Anholt, X.-Y. Xu, H. Gould, B. Feinberg, R. J. McDonald, H. E. Wegner, and P. Thieberger, Phys. Rev. A **35**, 1967 (1987).

[8] J. Eichler, Phys. Rev. A **32**, 112 (1985).

[9] A. Ichihara, T. Shirai, and J. Eichler, At. Data Nucl. Data Tables **55**, 63 (1993).

[10] Th. Stohlker, H. Geissel, H. Irnich, T. Kandler, C. Kozhuharov, P. H. Mokler, G. Munzenberg, F. Nickel, C. Scheidenberger, T. Suzuki, M. Kucharski, A. Warczac, P. Rymuza, Z. Stachura, A. Kriessbach, D. Dauvergne, B. Dunford, J. Eichler, A. Ichihara, and T. Shirai, Phys. Rev. Lett. **73**, 3520 (1994).

[11] Th. Stohlker, C. Kozhuharov, P. H. Mokler, A. Warczac, F. Bosch, H. Geissel, J. Eichler, A. Ichihara, T. Shirai, Z. Stachura, and P. Rymuza, Phys. Rev. A **51**, 2098 (1995).

[12] C. Scheidenberger, H. Geissel, Th. Stohlker, H. Folger, H. Irnich, C. Kozhuharov, A. Magel, P. H. Mokler, R. Moshammer, G. Munzenberg, F. Nickel, M. Pfutzner, P. Rymuza, W. Schwab, J. Ullrich, and B. Voss, Nucl. Instrum. Methods Phys. Res. B **90**, 36 (1994).

[13] B. Feinberg, Harvey Gould, W. E. Meyerhof, A. Belkacem, H.-P. Hulskotter, J. R. Alonso, L. Blumenfeld, E. Dillard, N. Guardala, G. F. Krebs, M. A. McMahan, M. J. Rhoades-Brown, B. S. Rude, J. Schweppe, D. W. Spooner, K. Street, P. Thieberger, and H. Wegner, Phys. Rev. A **47**, 2370 (1993).
[14] H.-P. Hulskotter, B. Feinberg, W. E. Meyerhof, A. Belkacem, J. R. Alonso, L. Blumenfeld, E. A. Dillard, H. Gould, N. Guardala, G. F. Krebs, M. A. McMahan, M. J. Rhoades-Brown, B. S. Rude, J. Schweppe, D. W. Spooner, K. Street, P. Thieberger, and H. E. Wegner, Phys. Rev. A **44**, 1712 (1991).
[15] H. Berg, R. Dörner, C. Kelbch, J. Ullrich, S. Hagmann, P. Richard, H. Schmidt-Böcking, A. S. Schlachter, M. Prior, H. J. Crawford, J. M. Engelage, I. Flores, D. H. Loyd, J. Pedersen, and R. E. Olson, J. Phys. B **21**, 3929 (1988).
[16] H. Berg, O. Jagutzki, R. Dörner, R. D. DuBois, C. Kelbch, H. Schmidt-Böcking, J. A. Tanis, A. S. Schlachter, L. Blumenfeld, B. d'Etat, S. Hagmann, A. Gonzales, and T. Quinteros, Phys. Rev. A **46**, 5539 (1992).
[17] D. Basu, S. C. Mucherjee, and D. P. Sural, Phys. Rep. **42C**, 145 (1978), and references therein.
[18] J. Eichler, Phys. Rep. **193**, 167 (1990).
[19] J. Eichler and W. E. Meyerhof, *Relativistic Atomic Collisions* (North-Holland, Amsterdam, 1995).
[20] J. M. Maidagan and R. D. Rivarola, J. Phys. B **17**, 2477 (1984).
[21] B. L. Moiseiwitsch, J. Phys. B **19**, 3733 (1986).
[22] N. Toshima and J. Eichler, Phys. Rev. A **38**, 2305 (1988).
[23] N. Toshima and J. Eichler, Phys. Rev. A **40**, 125 (1989).
[24] R. Anholt and U. Becker, Phys. Rev. A **36**, 4628 (1987).
[25] P. A. Amundsen and K. Aashamar, J. Phys. B **14**, 4047 (1981).
[26] S. R. Valluri, U. Becker, N. Grun, and W. Scheid, J. Phys. B **17**, 4359 (1984).
[27] G. Mehler, G. Soff, K. Rumrich, and W. Greiner, Z. Phys. D **13**, 193 (1989).
[28] J. Eichler, A. Ichihara, and T. Shirai, Phys. Rev. A **51**, 3027 (1995).
[29] P. Rymuza, Th. Stohlker, C. L. Cocke, H. Geissel, C. Kozhuharov, P. H. Mokler, R. Moshammer, F. Nickel, C. Scheidenberger, Z. Stachura, J. Ullrich, and A. Warczak, J. Phys. B **26**, L169 (1993).
[30] Andrew Westphal and Y. D. He, Phys. Rev. Lett. **71**, 1160 (1993).
[31] A. Belkacem, H. Gould, B. Feinberg, R. Bossingham, and W. E. Meyerhof, Phys. Rev. Lett. **71**, 1514 (1993).
[32] A. Belkacem, H. Gould, B. Feinberg, R. Bossingham, and W. E. Meyerhof, Phys. Rev. Lett. **73**, 2432 (1994).
[33] C. A. Bertulani and G. Baur, Phys. Rep. **163**, 299 (1988).
[34] F. Decker, Phys. Rev. A **44**, 2883 (1991).
[35] U. Becker, N. Grun, and W. Scheid, J. Phys. B **19**, 1347 (1986).
[36] C. Bottcher and M. R. Strayer, Phys. Rev. D **39**, 1330 (1989).
[37] D. C. Ionescu and J. Eichler, Phys. Rev. A **48**, 1176 (1993).
[38] K. Hencken, D. Trautmann, and G. Baur, Phys. Rev. A **51**, 1874 (1995).
[39] G. Baur, Phys. Rev. A **42**, 5736 (1990).
[40] P. B. Eby, Nucl. Instrum. Methods Phys. Res. B **336**, 189 (1993).
[41] M. Fatyga, M. J. Rhoades-Brown and M. J. Tannenbaum, Brookhaven National Laboratory Formal Report No. 52247, 1990 (unpublished).
[42] C. R. Vane, S. Datz, P. F. Dittner, H. F. Krause, C. Bottcher, M. Strayer, R. Schuch, H. Gau, and R. Hutton, Phys. Rev. Lett. **69**, 1911 (1992).
[43] C. R. Vane, S. Datz, P. F. Dittner, H. F. Krause, C. Bottcher, M. Strayer, R. Schuch, H. Gau, and R. Hutton, Phys. Rev. A **50**, 2313 (1994).
[44] J. H. Derrickson, P. B. Eby, K. H. Monn, T. A. Parnell, D. T. King, J. C. Gregory, Y. Takahashi, and T. Ogata, Phys. Rev. A **51**, 1253 (1995).
[45] R. Baur, A. Breskin, R. Checkik, A. Drees, U. Faschingbauer, P. Fischer, Z. Fraenkel, Ch. Fuchs, E. Gatti, J. Glaβ, P. Glassel, T. F. Gunzel, C. P. de los Heros, F. Heβ, D. Irmscher, C. Jacob, R. Manner, H. Manner, H. Nagele, K. H. Noffz, L. H. Olsen, A. Pfeiffer, I. Ravinovich, P. Rehak, M. Sampietro, B. Schmitt, A. Schon, J. Schukraft, C. Schwick, A. Shor, H. J. Specht, V. Steiner, S. Tapprogge, G. Tel-Zur, I. Tserruya, T. Ullrich, N. Waermes, A. Worner, and J. P. Wurm, Phys. Lett. B **332**, 471 (1994).
[46] G. L. Strobel and R. A. Koss, Int. J. Theor. Phys. **30**, 1235 (1991).
[47] P. L. Jain, M. Kazuno, B. Girard, and Z. Ahmad, Phys. Rev. Lett. **32**, 797 (1974).
[48] H. Gould, Lawrence Berkeley Laboratory Report No. LBL-18593, 1984.
[49] U. Becker, N. Grun, and W. Scheid, J. Phys. B **20**, 2075 (1987).
[50] K. Rumrich, K. Momberger, G. Soff, W. Greiner, N. Grun, and W. Scheid, Phys. Rev. Lett. **66**, 2613 (1991).
[51] K. Momberger, A. Belkacem, and A. H. Sorensen, Europhys. Lett. **32**, 401 (1995).
[52] K. Momberger, A. Belkacem, and A. H. Sorensen, Phys. Rev. A **53**, 1605 (1996).
[53] K. Momberger, N. Grun, and W. Scheid, Z. Phys. D **18**, 133 (1991).
[54] J. Thiel, A. Bunker, K. Momberger, N. Grun, and W. Sheid, Phys. Rev. A **46**, 2607 (1992).
[55] J. Thiel, J. Hoffstadt, N. Grun, and W. Scheid, Z. Phys. D **34**, 21 (1995).
[56] A. J. Baltz, M. J. Rhoades-Brown, and J. Weneser, Phys. Rev. A **44**, 5569 (1991).
[57] A. J. Baltz, M. J. Rhoades-Brown, and J. Weneser, Phys. Rev. A **47**, 3444 (1993).
[58] A. J. Baltz, M. J. Rhoades-Brown, and J. Weneser, Phys. Rev. A **48**, 2002 (1993).
[59] A. J. Baltz, M. J. Rhoades-Brown, and J. Weneser, Phys. Rev. A **50**, 4842 (1994).
[60] M. J. Rhoades-Brown, C. Bottcher, and M. R. Strayer, Phys. Rev. A **40**, 2831 (1989).
[61] C. Bottcher, M. J. Rhoades-Brown, and M. R. Strayer, Phys. Rev. A **44**, 4769 (1991).
[62] D. C. Ionescu, Phys. Rev. A **49**, 3188 (1994).
[63] U. Becker, J. Phys. B **20**, 6563 (1987).
[64] K. Rumrich, G. Soff, and W. Greiner, Phys. Rev. A **47**, 215 (1993).
[65] G. Deco and N. Grun, J. Phys. B **22**, 3709 (1989).
[66] G. Deco and D. Rivarola, J. Phys. B **22**, 1043 (1989).
[67] F. Decker and J. Eichler, Phys. Rev. A **44**, 2195 (1991).
[68] A. Aste, K. Hencken, D. Trautman, and G. Baur, Phys. Rev. A **50**, 3980 (1994).
[69] G. Baur *et al.*, Phys. Lett. B **368**, 251 (1996).
[70] BNL Report No. BNL-52195, May 1989, pp. 117–121. See especially Table IV. 3–10.

[71] D. C. Ionescu and J. Eichler, Phys. Rev. A **54**, 4960 (1996) and J. Eichler, Phys. Rev. Lett. **75**, 3653 (1995).

[72] H. D. Betz, Rev. Mod. Phys. **44**, 465 (1972); *Methods of Experimental Physics* (Academic, New York, 1980), Vol. 17, p. 73.

[73] J. H. Hubbell, in *Photon Cross Sections Attenuation Coefficients, and Energy Absorption Coefficients from 10 keV to 100 GeV*, edited by Editor(s), Natl. Bur. Stand. Ref. Data Ser., Natl. Bur. Stand. (U.S.) Circ. No. NSRDS-NBS 29 (U.S. GPO, Washington, DC, 1969).